


Cite this: *RSC Adv.*, 2024, 14, 101

# *In vitro* and *in vivo* studies of *Syzygium cumini*-loaded electrospun PLGA/PMMA/collagen nanofibers for accelerating topical wound healing

Esraa B. Abdelazim,<sup>a</sup> Tasneem Abed,<sup>a</sup> Shaimaa S. Goher,<sup>b</sup> Shaza H. Alya,<sup>c</sup> Heba A. S. El-Nashar,<sup>d</sup> Shahira H. EL-Moslami,<sup>e</sup> Esmail M. EL-Fakharany,<sup>f</sup> Enas A. Abdul-Baki,<sup>ag</sup> Marwa Mosaad Shakweer,<sup>hi</sup> Noura G. Eissa,<sup>aj</sup> Mahmoud Elsabahy<sup>\*ak</sup> and Elbadawy A. Kamoun<sup>ib\*lm</sup>

This work aims to develop plant extract-loaded electrospun nanofiber as an effective wound dressing scaffolds for topical wound healing. Electrospun nanofibers were fabricated from *Syzygium cumini* leaf extract (SCLE), poly(lactic-co-glycolic acid) (PLGA), poly(methyl methacrylate) (PMMA), collagen and glycine. Electrospinning conditions were optimized to allow the formation of nanosized and uniform fibers that display smooth surface. Morphology and swelling behavior of the formed nanofibers were studied. In addition, the antibacterial activity of the nanofibers against multidrug-resistant and human pathogens was assessed by agar-well diffusion. Results showed that nanofibers containing *Syzygium cumini* extract at concentrations of 0.5 and 1% w/v exhibited greater antibacterial activity against the tested Gram-positive (i.e., *Staphylococcus aureus*, *Candida albicans*, *Candida glabrata* and *Bacillus cereus*) and Gram-negative (i.e., *Salmonella paratyphi* and *Escherichia coli*) pathogens compared to the same concentrations of the plain extract. Furthermore, *in vivo* wound healing was evaluated in *Wistar* rats over a period of 14 days. *In vivo* results demonstrated that nanofiber mats containing SCLE and collagen significantly improved wound healing within two weeks, compared to the control untreated group. These findings highlight the potential of fabricated nanofibers in accelerating wound healing and management of topical acute wounds.

Received 19th September 2023  
Accepted 25th November 2023

DOI: 10.1039/d3ra06355k

rsc.li/rsc-advances

## 1 Introduction

Although the skin is capable of self-regeneration, wound healing is decelerated in cases of severe injuries and wounds.<sup>1</sup> The WHO reports that 265 000 people lose their lives each year as a direct result of wounds.<sup>2</sup> Nanomaterials of various types and compositions have been exploited for different applications

(e.g., antimicrobial, hemostatic and wound healing) owing to their ability to provide an enhanced surface area and stability for their loaded cargoes.<sup>3–7</sup> Of these, electrospun nanofibers (NFs) have demonstrated a wide range of applications in engineering, biology, and medicine.<sup>8,9</sup> For instance, NFs could provide significant ability to accelerate the healing process *in vivo* in several wound healing applications.<sup>10,11</sup>

<sup>a</sup>Badr University in Cairo Research Center, Badr University in Cairo, Badr City, Cairo 11829, Egypt. E-mail: mahmoud.elsabahy@buc.edu.eg

<sup>b</sup>Nanotechnology Research Centre (NTRC), The British University in Egypt (BUE), Suez Desert Road, El Sherouk City, Cairo 1183, Egypt

<sup>c</sup>Department of Pharmacognosy, Faculty of Pharmacy, Badr University in Cairo, Cairo, 11829, Egypt

<sup>d</sup>Department of Pharmacognosy, Faculty of Pharmacy, Ain Shams University, Cairo 11566, Egypt

<sup>e</sup>Bioprocess Development Dep., Genetic Engineering and Biotechnology Research Institute (GEBRI), City of Scientific Research and Technological Applications (SRTA-City), New Borg Al-Arab City 21934, Alexandria, Egypt

<sup>f</sup>Protein Research Dep., Genetic Engineering and Biotechnology Research Institute (GEBRI), City of Scientific Research and Technological Applications (SRTA-City), New Borg Al-Arab City 21934, Alexandria, Egypt

<sup>g</sup>Genomic Signature Cancer Center, Next Generation Sequencer Unit, Tanta University Global Educational Hospital, Tanta University, Tanta, Egypt

<sup>h</sup>Department of Pathology, Faculty of Medicine, Badr University in Cairo, Cairo, 11829, Egypt

<sup>i</sup>Department of Pathology, Faculty of Medicine, Ain Shams University, Cairo, Egypt

<sup>j</sup>Department of Pharmaceutics, Faculty of Pharmacy, Zagazig University, Zagazig 44519, Egypt

<sup>k</sup>Department of Chemistry, Texas A&M University, College Station, TX 77842, USA

<sup>l</sup>Polymeric Materials Research Dep., Advanced Technology and New Materials Research Institute (ATNMRI), City of Scientific Research and Technological Applications (SRTA-City), Alexandria 21934, Egypt

<sup>m</sup>Biomaterials for Medical and Pharmaceutical Applications Research Group, Nanotechnology Research Centre (NTRC), The British University in Egypt (BUE), Suez Desert Road, El Sherouk City, Cairo 1183, Egypt. E-mail: elbadawy.kamoun@bue.edu.eg



Electrospinning is a simple and economical approach utilized to develop fibers composed of natural (e.g., hyaluronic acid, gelatin, collagen, etc.) and/or synthetic polymers (e.g., poly(lactic-co-glycolic acid), poly(lactic acid), etc.) with diameters ranging from nanoscale to microscale.<sup>12</sup> Recently, electrospun nanofibrous wound dressings have received considerable interest for its high porosity, small-sized pores, and large surface area.<sup>13</sup> Poly(lactic-co-glycolic acid) (PLGA) is a synthetic FDA-approved polymer that is frequently used for biomedical applications due to its biocompatibility, biodegradability, and high mechanical strength.<sup>14,15</sup> Poly(methyl methacrylate) (PMMA) is an amorphous linear polymer that possesses excellent mechanical qualities and unique optical features.<sup>16</sup> Collagen (Col), a natural component of the extracellular matrix (ECM), has been described in the literature for developing nanofibrous scaffolds for tissue-engineering applications.<sup>17</sup> However, collagen is commonly combined with synthetic polymers that possess better mechanical properties for development of NFs to overcome its low mechanical strength.<sup>10</sup>

Incorporation of natural plant extracts (phytochemicals) that possess various therapeutic activities (e.g., antimicrobial, anti-inflammatory and wound healing) in the development of NFs provides an auspicious strategy towards achieving better therapeutic outcomes. *Syzygium cumini* (*S. cumini*) is one of the important genera in family Myrtaceae (Myrtle family).<sup>18</sup> Traditionally, different parts of *S. cumini* have been used for various applications. For example, fruits have been used to treat various conditions such as cough, diabetes, dysentery, inflammation, and ringworm.<sup>19</sup> Besides, traditional practitioners in India depend on *S. cumini* in different diseases as diarrhea, digestive complaints, dysentery, piles, and wound healing (pimples).<sup>20</sup> Furthermore, *S. cumini* demonstrated a plethora of pharmacological effects such as antioxidant, anti-inflammatory, antidiabetic and anti-allergic activities.<sup>21</sup> For example, the seeds of *S. cumini* revealed their effectiveness in elevation of glutathione levels that can be associated with high wound healing scores in laser-treated rats.<sup>22</sup>

In the current study, electrospun PLGA/PMMA/col/glycine NFs were designed to possess optimal properties (i.e., suitable mechanical strength, bioactive surface, and controllable degradability) and were loaded with *S. cumini* leaves extract (SCLE). The separation, characterizations, and structure identification of the SCLE, and the fabrication procedures of the electrospun NFs were described. The antimicrobial effects of the NFs, free and loaded with SCLE, against examples of Gram-positive and Gram-negative pathogens were assessed. Additionally, the wound healing activity of the therapeutic NFs was evaluated in an acute wound healing rat model.

## 2 Materials and methods

### 2.1 Materials

Poly(lactic-co-glycolic acid) (PLGA) with a lactide : glycolide ratio of 50 : 50, poly(methyl methacrylate) (PMMA,  $M_n \sim 550$  kDa), bovine collagen (col), glycine (gly) were obtained from Merck (Germany). Dichloromethane (DCM), *N,N*-dimethylformamide (DMF,  $\geq 99\%$  reagent grade) were obtained from Fisher

Chemicals (Belgium). All reagents were used as received without further purification.

The fresh leaves of *Syzygium cumini* were gathered from a private garden located in Abo-Zabal region (N 30°17'43.386", E 31°22'27.9804"), Qualioby, Egypt, in February 2021. The plant was authenticated by taxonomy proficient engineer from Labib, El-Orman Botanical Garden, Giza, Egypt. A voucher specimen was submitted at Pharmacognosy Department, Faculty of Pharmacy, Ain Shams University (voucher specimen number: PHG-P-SC-348).

The investigated multi-drug-resistant human pathogens were graciously donated by the Bioprocess Development Department, GEBRI, SRTA-City, Alexandria, Egypt. The chosen Gram-negative bacteria include *Salmonella paratyphi* (ATCC 9150) and *Escherichia coli* (ATCC 10536). Furthermore, some Gram-positive bacteria were utilized, such as *Bacillus cereus* (ATCC 19637) and *Staphylococcus aureus* (ATCC 25923). Moreover, *Candida albicans* (ATCC 10231) and *Candida glabrata* (ATCC 66032) were examined as fungal cells.

### 2.2 Extraction of defatted *Syzygium cumini*

The air-dried leaves of *S. cumini* (3 kg) were defatted through maceration in *n*-hexane (20 L) till exhaustion. The solvent was evaporated using a Rotavapor® (Hei-VAP value, Heidolph) under vacuum to obtain a dried residue (20 g). Then, the leaves were allowed to dry from remains of *n*-hexane followed by percolation in 80% methanol (20 L) for 72 h, followed by filtration. The filtrate was concentrated under vacuum (50 °C) till dryness using a Rotavapor® and the extract was subjected to lyophilization using a lyophilizer (Alpha 1–2 LD plus lyophilizer) to get rid of residual water and give ca. 450.23 g (extraction yield 16% w/w) of the total methanol SCLE. The yield (%) was obtained according to eqn (1):

$$\text{Yield}(\%) = \frac{\text{total weight of dried extract}}{\text{total weight of fresh plant}} \times 100. \quad (1)$$

The dried extract was retained in a tight sealed container at 20 °C for further investigations.

### 2.3 Fabrication of PLGA/PMMA/col/gly/SCLE nanofiber scaffolds

**2.3.1 Optimization of electrospun PLGA/PMMA/col NFs.** Separate solutions of PLGA (15% w/v) and PMMA (10% w/v) were initially prepared by dissolving in a DCM : DMF (7 : 3, v/v) binary solvent mixture. The polymer solutions of PLGA and PMMA were then blended in various volume ratios (4 : 1, 3 : 2, and 1 : 1, v/v) resulting in a polymer blend solution. The solutions were stirred at a constant speed of 500 rpm for 2 h at 60 °C. Later, col (1% w/v) was added to the mixtures and was stirred overnight at 60 °C and 500 rpm to ensure uniform dispersion. NFs were fabricated from PLGA/PMMA/col solutions using an electrospinner (MECC, NANON-01A, MECC, Japan) to determine the optimal spinning conditions. The homogeneous mixtures were loaded into a 5 mL syringe (22 G needle). Various electrospinning parameters were adjusted as shown in Table 1,



**Table 1** Lists the formulation codes, constituents, concentrations, and spinning conditions optimization for PLGA/PMMA/col/gly/SCLE nano-fiber scaffolds

Formulation no.	PLGA : PMMA (ratio)	PLGA (% w/v)	PMMA (% w/v)	Col (% w/v)	Gly (% w/v)	SCLE (% w/v)	Stirring time	Voltage (kV)	Feed rate (mL h <sup>-1</sup> )
F1	4 : 1	15	10	—	—	—	Overnight	16	0.8
F2	3 : 2	15	10	1	—	—	2 h	17	0.7
F3	4 : 1	15	10	1	—	—	2 h	16	0.6
F4	1 : 1	15	10	1	—	—	Overnight	17	0.8
F5	3 : 2	15	10	1	—	—	Overnight	17	0.8
F6	4 : 1	15	10	1	—	—	Overnight	17	0.8
F7	4 : 1	15	10	1	0.1	—	Overnight	22	0.8
F8	4 : 1	15	10	1	0.25	—	Overnight	22	0.8
F9	4 : 1	15	10	1	0.5	—	Overnight	22	0.8
F10	4 : 1	15	10	1	0.1	0.5	Overnight	20	0.6
F11	4 : 1	15	10	1	0.1	1	Overnight	22	0.4

including the feeding rate (ranging from 0.4 to 0.8 mL h<sup>-1</sup>), applied voltage (16–22 kV), and the tip-to-collector distance set at 13.5 cm.<sup>23</sup>

**2.3.2 Fabrication of PLGA/PMMA/col/gly and PLGA/PMMA/col/gly/SCLE NFs.** Glycine was added to the optimum polymer solution (80 : 20) at three concentrations (0.1, 0.2, and 0.5% w/v) to ensure even dispersion throughout PLGA/PMMA/col solution. Next, a well-distributed PLGA/PMMA/col/gly solution was prepared by stirring the mixture overnight at 60 °C. The resultant mixtures were electrospun at 22 kV applied voltage, 0.8 mL h<sup>-1</sup> feed rate, 60 cm spinneret width, and 13.5 cm spinneret distance using the previously adjusted settings as shown in Table 1.

PLGA/PMMA/col/gly/SCLE NFs were prepared by dissolving SCLE in the PLGA/PMMA (4 : 1)/col/gly (0.1% w/v) solution at room temperature and overnight stirring. The extract was added at concentrations of 0.5 and 1% (w/v). The SCLE-loaded PLGA/PMMA/col/gly solutions were electrospun (applied voltage of 23 kV and feed rate of 0.6 mL h<sup>-1</sup>) and collected on a width of 60 mm on a rectangle plate collector fixed at a distance of 13.5 cm from a 22 G needle. All electrospinning experiments were carried out at ambient conditions with a relative humidity of 40%. The optimization conditions of spinning parameters (e.g., polymers ratio, feeding rate of polymeric solution and the distances of spinning) were discussed in detail and presented in Table 2. The resultant nanofibers were stored at 4 °C for further use and experiments.

## 2.4 Characterization

**2.4.1 HPLC-MS/MS analysis.** Using HPLC coupled to ESI-MS, the phytochemical profiling of methanol extract of *S. cumini* leaves was conducted based on a recently published method,<sup>24,25</sup> that allows the determination of the molecular weight of the isolated peak. In summary, the extract was melted in HPLC grade methanol (100 µg mL<sup>-1</sup>), filtered using a membrane disc filter (0.2 µm) and injected in volume of 10 µL. The HPLC instrument (Acquity, Waters®, Milford, MA USA) was equipped with reversed-phase Acquity UPLC-BEH C<sub>18</sub> column (1.7 µm particle size, 2.1 × 50 mm). Mobile phase elution flow rate was adjusted to 0.2 mL min<sup>-1</sup> with a gradient of acidified

water with 0.1% formic acid and acidified methanol with 0.1% formic acid through a run that lasted for 35 min. ESI-MS in positive and negative ion acquisition modes was conducted on a XEVO TQD triple quadrupole instrument. The triple quadrupole mass spectrometer XEVO TQD was used for the mass spectrometric analysis (Waters Corporation, Milford, MA, USA) under the following conditions: 30 eV cone voltage, and 3 kV capillary voltage at 150 °C source temperature and 510 °C dissolution temperature using vacuum pump Edwards® (Chandler, AZ, USA). The mass spectra detection was carried out in ESI range of 100–1000 *m/z* using Maslynx 4.1, and the peaks were tentatively characterized through comparing their mass spectra and their fragmentation pattern with the reported data.

**2.4.2 SEM investigation.** To analyze the surface characteristics of blended electrospun nanofibers (NFs), scanning electron microscopy (SEM) investigation was performed by using a field emission environmental scanning electron microscope “FE-SEM” (Quattro S, Thermo Scientific USA). The samples were imaged without the application of any coatings to ensure accurate representation. To maintain the integrity of the samples, a 5 kV accelerating voltage was employed for microstructural and morphological evaluation of the electrospun fibers. Image J software was utilized for image analysis.

**2.4.3 FT-IR analysis.** To analyze the chemical composition of the PLGA/PMMA/col/gly/SCLE nanofiber scaffolds, Fourier transform infrared spectroscopy (FT-IR) was analyzed by FT-IR instrument (model 8400s, Shimadzu, Japan). Spectral data were recorded within a spectrum range of 4000–400 cm<sup>-1</sup> to obtain characteristic fingerprints and gain insights into the molecular composition of the scaffolds.

**2.4.4 X-ray diffraction analysis.** X-ray diffraction (XRD) patterns of the fabricated NFs were obtained using a (Malvern PANalytical, England, UK) diffractometer with Cu Kα radiation. The diffraction data were collected at 2θ ranged 5–60° with a step size of 0.02 and 0.5 s per step. XRD analysis was conducted in Bragg–Brentano mode. To ensure the samples were flat and properly positioned, the electrospun specimens were mounted on aluminum disks using tape.

**2.4.5 Swelling properties and *in vitro* degradation.** To assess the swelling properties of the developed scaffolds, all

Table 2 Spinning conditions optimization for PLGA/PMMA/Col nanofiber scaffolds

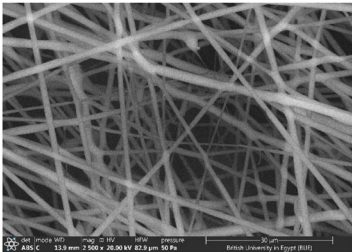
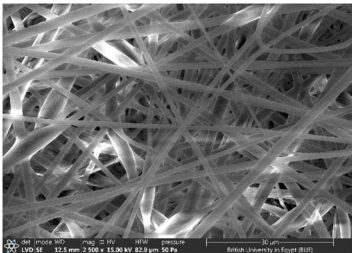
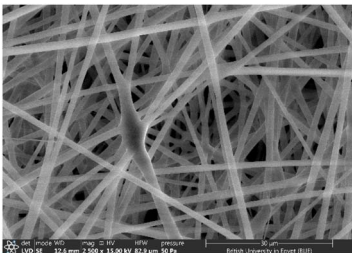
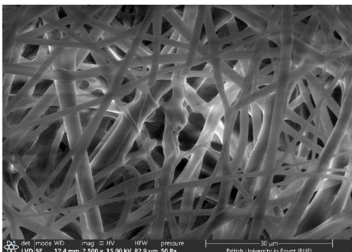
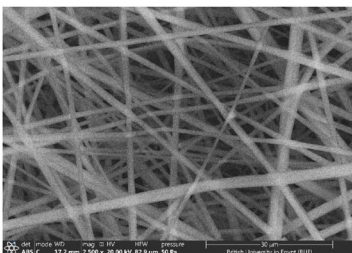
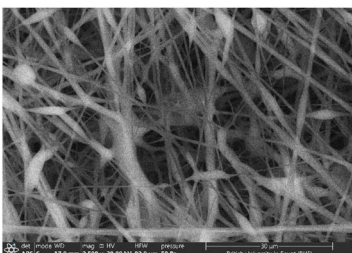
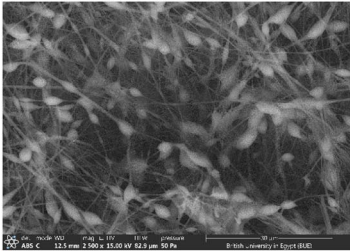
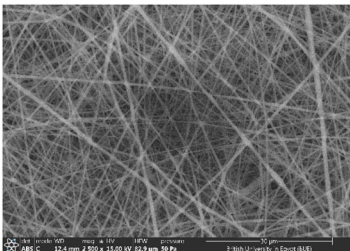
Formulations	PLGA : PMMA (ratio)	PLGA (% w/v)	PMMA (% w/v)	Col (% w/v)	Gly (% w/v)	SCLE (% w/v)	SEM images	Observation
F1	4 : 1	15	10	—	—	—		Uniform NFs
F2	3 : 2	15	10	1	—	—		No encapsulation
F3	4 : 1	15	10	1	—	—		Crosslinking No encapsulation
F4	1 : 1	15	10	1	—	—		Swollen diameter Encapsulated collagen
F5	3 : 2	15	10	1	—	—		No encapsulation
F6	4 : 1	15	10	1	—	—		Encapsulated collagen Crosslinking





Table 2 (Contd.)

Formulations	PLGA : PMMA (ratio)	PLGA (% w/v)	PMMA (% w/v)	Col (% w/v)	Gly (% w/v)	SCLE (% w/v)	SEM images	Observation
F7	4 : 1	15	10	1	0.1	—		Encapsulation
F8	4 : 1	15	10	1	0.25	—	No SEM investigated	Encapsulation Uniform NFs
F9	4 : 1	15	10	1	0.5	—	No SEM investigated	
F10	4 : 1	15	10	1	0.1	0.5	No SEM investigated	
F11	4 : 1	15	10	1	0.1	1		

tested samples were cut into (1 × 1 cm) (length × width) and soaked in deionized water at 37 °C for 48 h, removed at various time intervals and weighed. The wet ( $W_e$ ) and dry ( $W_d$ ) weights of the scaffolds were determined as described previously.<sup>26</sup> The excess moisture on the surface was extracted using filter paper each time. Swelling ratio (SR) was calculated using eqn (2):

$$SR(\%) = \frac{W_e - W_d}{W_d} \times 100. \quad (2)$$

**2.4.6 Evaluation of antimicrobial activity of scaffolds.** An agar-well diffusion test was utilized to assess the antimicrobial effects of the developed NFs,<sup>27</sup> which were coded in Table 1. The culture suspension ( $1 \times 10^6$  spores per mL) was swapped onto the nutrient agar plates. After that, 6 mm-diameter holes were drilled using specialized cork metal, and 50  $\mu$ L of the tested formulation were loaded individually within the holes. *S. cumini* extract at the two tested concentrations (0.5 and 1%) were independently examined as positive controls. The agar plates were statically incubated for 48 h at the proper temperature. After that, the inhibitory zones around the holes were measured. The data was collected from three independent experiments. The results were given as means with standard deviations. To statistically analyze the findings, Minitab software (Minitab® 18.1, 2017) was used for a one-way analysis of variance (ANOVA) with a  $p$ -value <0.05.

**2.4.7 In vitro cytotoxicity assay.** The *in vitro* cytotoxicity of the prepared NFs was studied by utilizing colorimetric methyl thiazolyl tetrazolium (MTT) method against normal kidney cells of an African green monkey (Vero cell line). Vero cells were cultured in a 96-well plate at a concentration of  $1.0 \times 10^4$  cells

per well and incubated for 24 h in 5% CO<sub>2</sub> incubator. NFs were soaked in phosphate buffer saline (PBS) for 48 h prior to being added to the cells at different concentrations (0.1, 0.2, 0.4, 0.6 and 0.8 mg mL<sup>-1</sup>) and incubated for an additional 72 h. After the incubation period, the cell media were removed, and the cells were washed three times with PBS. Then, 200  $\mu$ L of MTT (0.5 mg mL<sup>-1</sup>) were added to each well and the cells were further incubated for an additional 3 h. The resulting MTT-formazan formed layer by the viable cells was dissolved in 200  $\mu$ L of dimethyl sulfoxide (DMSO) and the absorbance was measured using an *iMark* microplate ELISA reader at 570 nm. The relative cell viability (%) was calculated as compared to the untreated control cells.

**2.4.8 In vivo wound healing assay.** The *in vivo* experiments were ethically approved by Badr University in Cairo-Institutional Ethical Committee No. (BUC-IACUC-230507-19). Twelve female Wistar rats (230–250 g) have been divided randomly into three groups, four animals each. At room temperature and a 12 hour light/dark life cycle, the animals were housed in a standard animal house that was equipped with cages and soft wood pellets for bedding. The rats were anesthetized with ketamine injection followed by hair removal.<sup>28</sup> Wounds were created on the dorsal surface of each rat skin by a 1 cm<sup>2</sup> biopsy punch. Surgical gauges were applied to all rats and kept back in their cages to avoid infection. Group 1 received no treatment and served as a control. Group 2 was treated with F7, and Group 3 was treated with F11. After 3, 6, 9, 12, and 14 d, the wound dressings were removed, and the diameter of wounds was measured with a caliper. The wound healing (%) was assessed according to eqn (3):



$$\text{Wound heading \%} = \frac{A_i - A_d}{A_i} \times 100 \quad (3)$$

where,  $A_d$  and  $A_i$  are the wound areas on the specified day and day zero, respectively. The rats in the 1st and 3rd group were sacrificed on day 14. To preserve the skin samples for later histological analysis, they were immediately placed in 10% formalin.

**2.4.9 Histological analysis.** Biopsy samples were fixed in 10% phosphate buffer formalin and paraffin sections (3–5 mm) were prepared. Sections were used for Hematoxylin and Eosin stain (H&E) and were investigated by a light microscope (Olympus, BH-2, Tokyo, Japan).<sup>29</sup> Stage 1: assessment of inflammatory phase: macrophages, mast cells, lymphocytes, and neutrophils. Stage 2: granulation tissue formation: blood vessels to evaluate angiogenesis, fibroblasts and collagen. Stage 3: the assessment of collagen fibers regarding amount and orientation role during the remodeling phase. Stage 4: assessment of the final scar at the end of wound healing.

**2.4.10 Statistical analysis.** All the outcomes were evaluated through *t*-tests or one-way analysis of variance (ANOVA). Findings with *p*-values below 0.05 were regarded as statistically significant. The statistical analysis was carried out using version 8 of GraphPad Prism software.

## 3 Results and discussion

### 3.1 HPLC-ESI-MS/MS analysis of phytoconstituents of SCLE

HPLC-ESI-MS/MS analysis was utilized to investigate the phytoconstituents in the methanol extract of *S. cumini* leaves. The total ion chromatogram (TIC) in negative and positive

ionization modes is shown in Fig. 1. A total of 27 phenolic compounds belonging to different classes as flavonoids, lignans, tannins, anthocyanins and phenolic acids have been identified tentatively through evaluation of their MS characteristics and fragmentation pattern and compared to earlier reported findings on *S. cumini* (Table 3). The most predominant class of secondary metabolites was the flavonoid glycosides, especially the hexose conjugates as well as the anthocyanins.

The ion mass peaks at  $m/z$  463, 505, 451 and 479 for the suggested molecular formulae  $C_{21}H_{20}O_{12}$ ,  $C_{23}H_{22}O_{13}$ ,  $C_{20}H_{18}O_{12}$  and  $C_{21}H_{20}O_{13}$ , respectively, corresponds to the characterized myricetin compounds (4, 6, 11 and 21). Myricetin glycoside was reported for its *in vitro* potential wound healing properties through efficient fibroblast migration and high rate of wound closure and enhancement of cell proliferation.<sup>30</sup> Another *in vivo* study revealed the efficiency of myricetin in promoting the wound closure in treated rats.<sup>31</sup> Besides, two ion peak values at  $m/z$  449 and 593 with molecular formulae  $C_{21}H_{20}O_{11}$  and  $C_{27}H_{30}O_{15}$ , respectively, were tentatively identified as kaempferol glycosides in (10 and 12). Kaempferol was reported for its wound healing and antioxidant properties for normal and diabetic wounds. This might be because of the capacity to scavenge free radicals, enhanced cross-linking, and higher protein contents in treated animals, in addition to enhanced wound healing through higher levels of hydroxyproline and enhancement of re-epithelialization.<sup>32</sup>

Moreover, apigenin glycoside was characterized with ion peak value at  $m/z$  431 in (3) that may enhance the re-epithelialization and wound contraction and reduce wound size.<sup>33,34</sup> It has a potency in promoting wound closure through

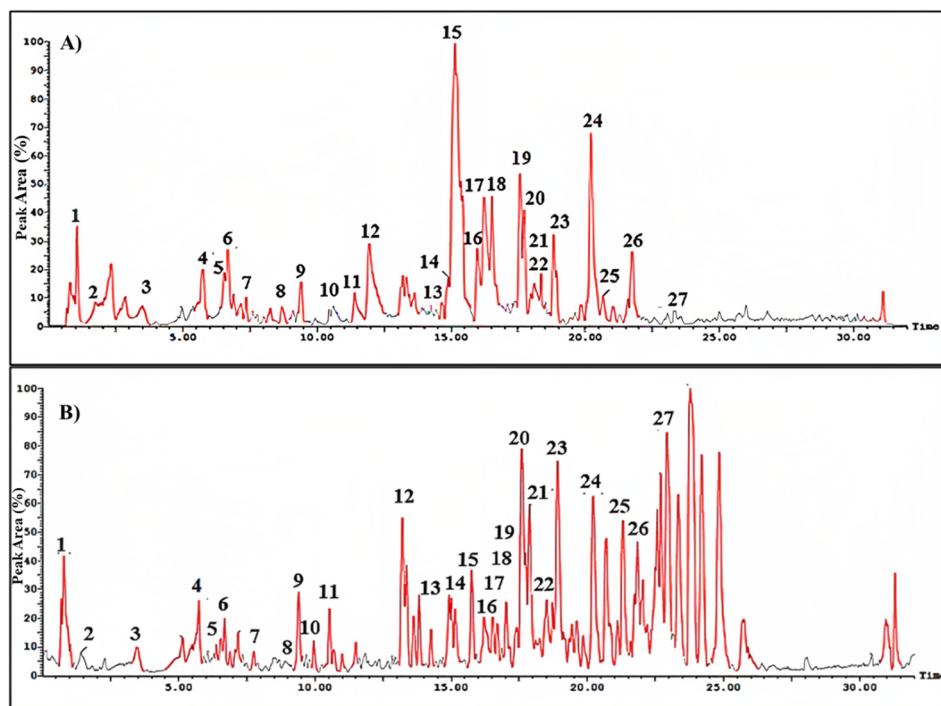


Fig. 1 Total ion chromatogram (TIC) for methanol extract of *Syzygium cumini* leaves in negative (A) and positive (B) ionization modes. The numbers assigned to the peaks are explained in Table 3.



Table 3 Characteristics of *Syzygium cumini* phytoconstituents identified by HPLC-MS/MS in the positive and negative ionization mode

Peak no.	Compound name	$t_R$ (min)	Molecular formula	Molecular weight	$m/z$ detected and adduct	$MS^2$ fragments	Chemical class	Ref.
1	Gallic acid	1.02	$C_7H_6O_5$	170	$169[M - H]^-$	125, 107, 69, 51	Phenolic acids	40
2	Corilagin	1.74	$C_{27}H_{22}O_{18}$	634	$633[M - H]^-$	315, 301, 265	Ellagitannins	41
3	Apigenin- <i>O</i> -hexoside	3.45	$C_{21}H_{20}O_{10}$	432	$431[M - H]^-$	269	Flavonoids	42
4	Myricetin- <i>O</i> -deoxyhexoside	5.74	$C_{21}H_{20}O_{12}$	464	$463[M - H]^-$	462, 446, 316, 124	Flavonoids	41
5	Monogalloylglucose	6.38	$C_{13}H_{16}O_{10}$	332	$333[M + H]^+$	271, 169, 125, 108	Gallotannins	41
6	Myricetin- <i>O</i> -acetylramnoside	6.69	$C_{23}H_{22}O_{13}$	506	$505[M - H]^-$	316, 217	Flavonoids	43
7	Delphinidin- <i>O</i> -gentiobioside	7.18	$C_{27}H_{31}O_{17}^+$	627	$626[M - H]^-$	465, 303	Anthocyanins	44
8	Bergenin	8.70	$C_{14}H_{16}O_9$	328	$327[M - H]^-$	234, 207, 192	Iso-coumarin	45
9	Citric acid	9.40	$C_6H_8O_7$	192	$193[M + H]^+$	173, 127, 111	Organic acids	46
10	Kaempferol- <i>O</i> -hexoside	9.96	$C_{21}H_{20}O_{11}$	448	$449[M + H]^+$	284, 255, 227	Flavonoids	47
11	Myricetin- <i>O</i> -pentoside	11.00	$C_{20}H_{18}O_{12}$	450	$451[M + H]^+$	316	Flavonoids	45
12	Kaempferol- <i>O</i> -robinobioside	13.20	$C_{27}H_{30}O_{15}$	594	$593[M - H]^-$	285	Flavonoids	47
13	Syringaresinol- <i>O</i> -hexoside	14.65	$C_{28}H_{36}O_{13}$	580	$579[M - H]^-$	417, 402, 295, 166	Lignans	48
14	Pinoresinol- <i>O</i> -hexoside	14.92	$C_{26}H_{32}O_{11}$	520	$521[M + H]^+$	357, 342, 151, 136	Lignans	49
15	Delphinidin- <i>O</i> -hexoside	10.53	$C_{21}H_{21}O_{12}^+$	465	$466[M + H]^+$	303, 257, 173	Anthocyanins	50
16	Cyanidin- <i>O</i> -hexoside	15.97	$C_{21}H_{21}O_{11}^+$	484	$483[M + H]^-$	327, 287, 255	Anthocyanins	51
17	Pentahydroxyflavone; taxifolin	16.21	$C_{15}H_{12}O_7$	304	$303[M - H]^-$	285, 275, 177, 125	Flavonoids	42
18	Malvidin- <i>O</i> -hexoside- <i>O</i> -deoxyhexoside; malvidin- <i>O</i> -laminaribioside	16.54	$C_{29}H_{35}O_{17}^+$	655	$654[M - H]^-$	493, 329, 315	Anthocyanins	52
19	Petunidin- <i>O</i> -dihexoside; Petunidin- <i>O</i> -gentiobioside	17.14	$C_{28}H_{33}O_{17}^+$	641	$642[M + H]^+$	479, 315, 314, 216	Anthocyanins	44
20	Malvidin- <i>O</i> -hexoside	17.73	$C_{23}H_{25}O_{12}^+$	493	$494[M + H]^+$	329, 315	Anthocyanins	53
21	Myricetin- <i>O</i> -hexoside	17.97	$C_{21}H_{20}O_{13}$	480	$479[M - H]^-$	472, 462, 316, 271	Flavonoids	53
22	Hydroxypinoresinol	18.35	$C_{20}H_{22}O_7$	374	$373[M - H]^-$	342, 311, 175	Lignans	54
23	Pinoresinol	18.90	$C_{20}H_{22}O_6$	358	$357[M - H]^-$	342, 311, 175, 136	Lignans	54
24	Dimethylpinoresinol ether	20.70	$C_{22}H_{26}O_6$	386	$385[M - H]^-$	369, 358, 297	Lignans	54
25	Cyanidin- <i>O</i> -di-hexoside	21.10	$C_{27}H_{31}O_{16}^+$	611	$612[M + H]^+$	484, 287, 258, 241	Anthocyanins	52
26	Jambone G	21.73	$C_{26}H_{36}O_4$	412	$413[M + H]^+$	178	Chromones	52
27	Isorhamnetin- <i>O</i> -rutinoside	22.92	$C_{28}H_{32}O_{16}$	624	$623[M - H]^-$	315, 300, 271	Flavonoids	51

its anti-inflammatory and antioxidant properties.<sup>35</sup> Another flavonoid with molecular ion peak of 623 and molecular formula  $C_{28}H_{32}O_{15}$  corresponding to isorhamnetin-*O*-rutinoside (27) showed a major decrease in the scratch area *in vitro* as well as *in vivo* model of burn wounds and resulted in the suppression of inflammatory mediators such as IL-1 $\beta$ , IL-6 and Bcl-2 as well as elevation of matrix metalloproteinase 9, transforming growth factor  $\beta$ , and vascular endothelial growth factor.<sup>36</sup> Six anthocyanins were identified in SCLE (7, 15, 16, 18, 19 and 25) that were reported for their wound healing potential ascribed to their antioxidant and anti-inflammatory activities.<sup>37</sup> Moreover, five lignans were identified in SCLE (13, 14 and 22–24) that were reported for their antioxidant activity and thus wound healing properties.<sup>38</sup> Tannins in SCLE are represented as ellagitannins (2) and gallotannins (5) that have been proven to be useful in wound healing and scar re-modelling through their tendency to induce vascular development.<sup>39</sup> The chemical structures of the major compounds present in SCLE are demonstrated in Fig. 2.

### 3.2 SEM investigation

Several optimization procedures were performed to select the optimal PLGA/PMMA ratio for fabrication of NFs as shown in Table 2. NFs prepared utilizing PLGA/PMMA at a ratio of 4 : 1 displayed smooth and beads-free nanofibers, thus, was selected

for further preparations. The surface morphology of the fabricated NFs is demonstrated in Fig. 3A–D. Prior to the addition of collagen, PLGA/PMMA nanofibers displayed smooth surface without beads formation (Fig. 3A1). Collagen addition altered the surface properties of the formed nanofibers (Fig. 3B1), in agreement with previous work by other groups,<sup>55,56</sup> with no change in the fiber diameter. Addition of gly resulted in the formation of a thinner fiber (0.96  $\mu$ m thickness) (Fig. 3C2) that was further reduced upon incorporation of the SCLE (0.48  $\mu$ m thickness) (Fig. 3D2). Whereas encapsulation does not occur when PMMA concentration increases, as seen in Table 2.

### 3.3 FT-IR analysis

The FT-IR spectrum revealed the presence of asymmetric stretching peaks of C–H bond in the  $-CH_2-$  and  $-CH-$  groups of an aliphatic chain of PLGA which were found as weak signals at 2990 and 2953  $cm^{-1}$ . Furthermore, a strong signal at 1741  $cm^{-1}$  was observed due to the stretching of the C=O bond in the ester group. In addition, stretching of C–O single bonds in the ester group was reflected in the signals at 1170, 1450, and 1076  $cm^{-1}$ , demonstrating common peaks of PLGA.<sup>57</sup> PMMA spectrum showed a sharp peak at 1722  $cm^{-1}$  that corresponds to C=O stretching, a peak at 1187  $cm^{-1}$  that is attributable to C–O bond in ester group and a stretching vibration of  $CH_3$  groups at around 2993 and 2948  $cm^{-1}$ . Other peaks observed at 1266 and



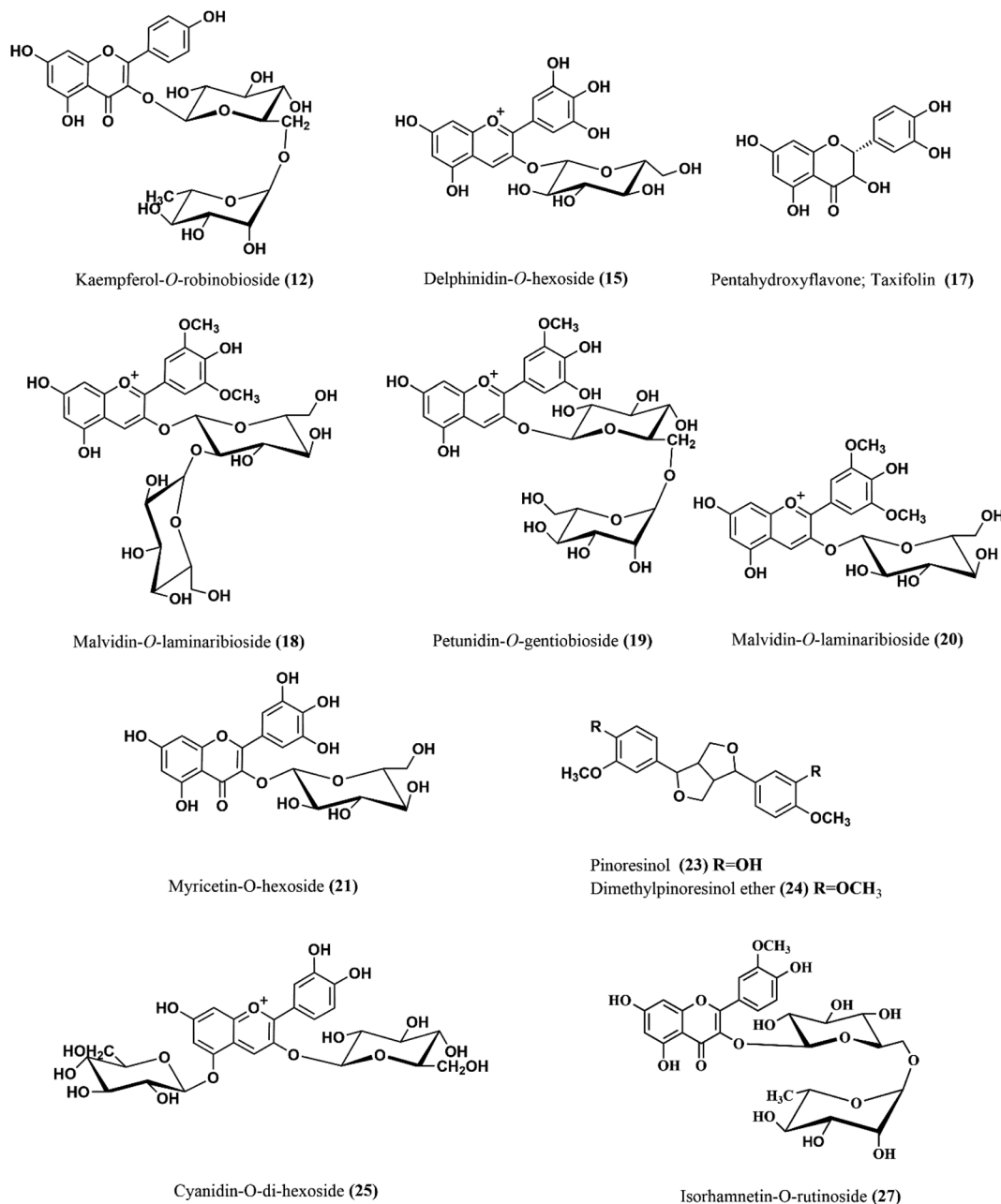


Fig. 2 The chemical structures of major compounds of the SCLE identified by HPLC-MS/MS. SCLE: *S. cumini* leaves extract.

1240  $\text{cm}^{-1}$  correspond to C–C–O bonds in ester group, and at 1475 and 1436  $\text{cm}^{-1}$  indicate skeletal  $\text{CH}_2$  deformation. Additionally, peaks at 1186 and 1140  $\text{cm}^{-1}$  were attributed to C–O–C vibrations of methoxy group.<sup>26</sup> Collagen spectrum showed N–H stretching and O–H stretching displaying a broad, strong absorption peak at 3284  $\text{cm}^{-1}$  which is attributed to amide A band absorption. Two more weak absorption peaks were also observed at 3065  $\text{cm}^{-1}$  (C–N stretching) and 3931  $\text{cm}^{-1}$  ( $\text{CH}_2$  asymmetric stretching). Absorption peaks were detected between 1700 and 1200  $\text{cm}^{-1}$  and at 1632  $\text{cm}^{-1}$  (amide I band absorption, associated with C–O stretching and hydrogen bonding), 1527  $\text{cm}^{-1}$  (amide II band absorption, linked to NH bending vibration and CN stretching), and 1237  $\text{cm}^{-1}$  (amide III

band absorption, related to NH bending vibration). The amides I, II, and III peaks are excellent indicators of the structure of protein polypeptides. Also, collagen 3-screw structure is shown to be highly correlated with 1440–1237  $\text{cm}^{-1}$  absorption peaks. The spectrum of SCLE showed prominent peaks at different wavenumbers at 3300, 2929, 1714, 1447, 1350, 1033 and 583  $\text{cm}^{-1}$ . Specifically, the peak that was detected at 3300  $\text{cm}^{-1}$  indicates the stretching vibration of hydroxyl group (–OH) which characterizes a polyphenolic molecule and corresponds to the intermolecular hydrogen bond for O–H of carboxylic acid, alcohols, and phenols.<sup>58</sup> The absorbance band at 2929  $\text{cm}^{-1}$  revealed the asymmetrical stretching vibration in C–H bond. In addition, peaks at 1694  $\text{cm}^{-1}$  and 1030  $\text{cm}^{-1}$  are ascribed to





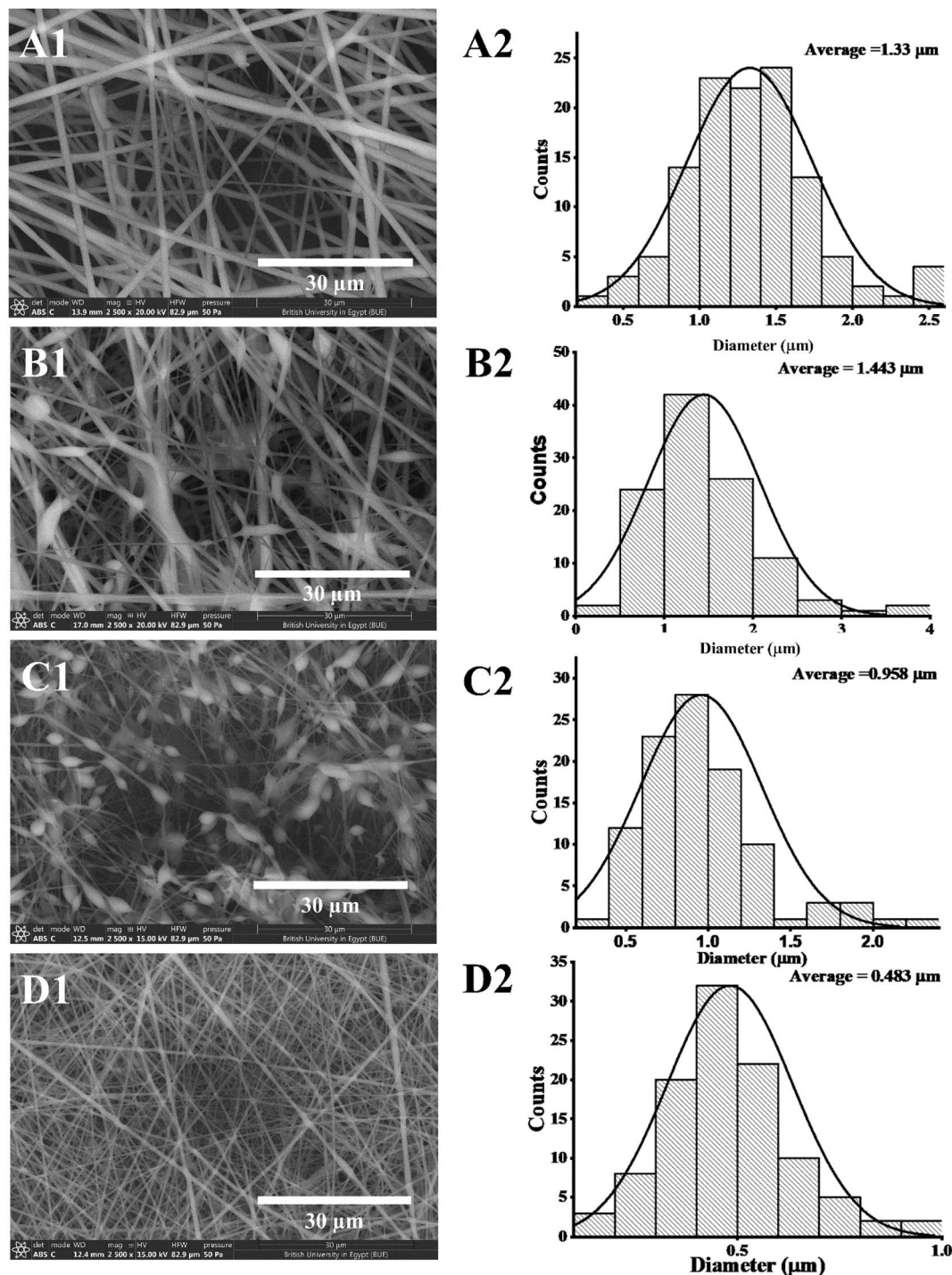


**Fig. 3** Scanning electron microscopy images, captured at a magnification of 2500 $\times$ , showing the morphology of electrospun PLGA/PMMA/col/gly/SCLE nanofibers: (A1) PLGA (15%)/PMMA (10%) (F1), (B1) PLGA/PMMA/col (1%) (F6), (C1) PLGA/PMMA/col/gly (0.1%) (F7), and (D1) PLGA/PMMA/col/gly (0.1%)/SCLE (1%) (F11). A2, B2, C2, and D2 represent diameter distribution histograms of F1, F6, F7, and F11, respectively.

carbonyl (C=O) stretching vibration and C–O single bonds. The peak at 1447  $\text{cm}^{-1}$  indicates the presence of aromatic C=C and peaks at 1350 and 1030  $\text{cm}^{-1}$  are owing to C–O–C stretching vibrations of alcohols and C–O–C ether bonds of heterocyclic ring. All mentioned peaks confirmed the presence of different secondary metabolites components in SCLE (tannins, flavonoids, anthocyanins, and phenolic acids). The FT-IR analysis is

in correlation with previously reported FTIR findings of *S. cumini* (Fig. 4).<sup>59</sup>

### 3.4 XRD analysis

XRD analysis was performed to further elucidate the structure of PLGA/PMMA/col/gly/SCLE NFs (F11) and for better understanding of their crystalline properties (Fig. 5). XRD pattern of



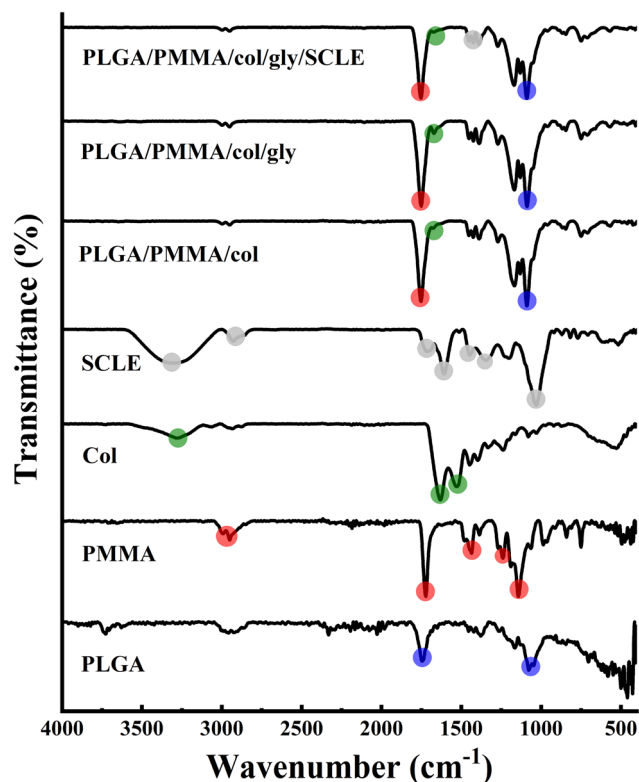


Fig. 4 FTIR spectra of individual components of the electrospun PLGA/PMMA/col/gly/SCLE nanofibers. The main characteristic peaks of each spectrum are highlighted to demonstrate changes in the formed nanofibers.

PLGA showed no obvious peaks, suggesting its amorphous nature. Similarly, a wide peak at  $2\theta$   $18.1^\circ$  was demonstrated for pure PMMA, which is consistent with previously reported data.<sup>60</sup> Remarkably, collagen component in PLGA/PMMA/col/gly/SCLE NFs (F11) maintained its amorphous phase, as evidenced by the absence of discrete peaks (Fig. 5). This finding indicates that F11 maintained the amorphous nature of collagen. XRD pattern of F11 illustrated the incorporation of SCLE peak into the NFs.

### 3.5 Swelling study

Swelling index of electrospun nanofiber has a crucial role in the drug loading and release behaviour. Fig. 6 illustrates the time-dependent swelling of SCLE-loaded (F11), PLGA/PMMA/col/gly (F7), and PLGA/PMMA/col (F6) NFs. The swelling ratio for F6 in PBS pH 7.4 showed the highest swelling (125%) after 48 h. Lower swelling ratio was observed in case of F11 as compared to F7 which might be attributed to the release of the plant extract from the fabricated NFs.

### 3.6 *In vitro* evaluation of antimicrobial effectiveness of tested formulations

There must be more efforts to solve the serious issue of pathogen resistance to commonly prescribed antibiotics. The use of medicinal plants can be considered a useful alternative for antimicrobial agents.<sup>61</sup> *S. cumini* extracts demonstrated remarkable pharmacological and antimicrobial activities.<sup>62</sup> The promising therapeutic activity of *S. cumini* extracts can be

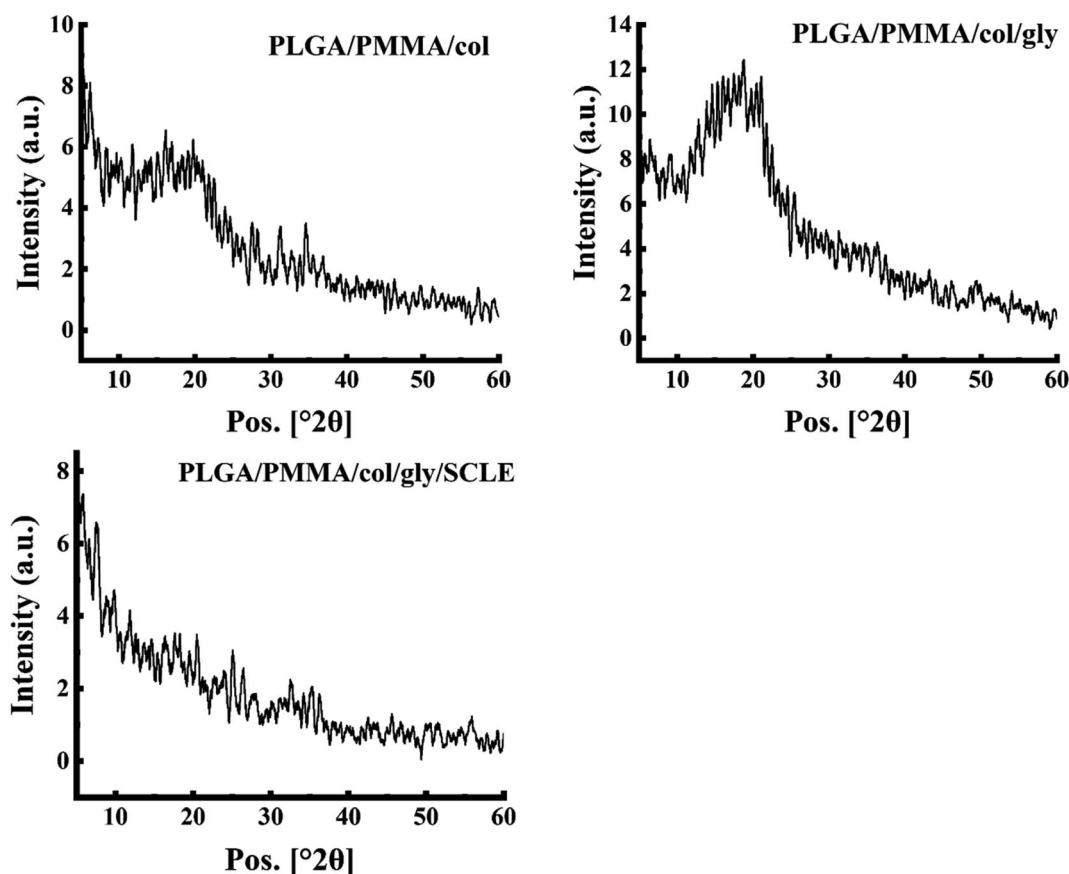


Fig. 5 XRD patterns of components of electrospun PLGA/PMMA/col/gly nanofibers loaded with SCLE.



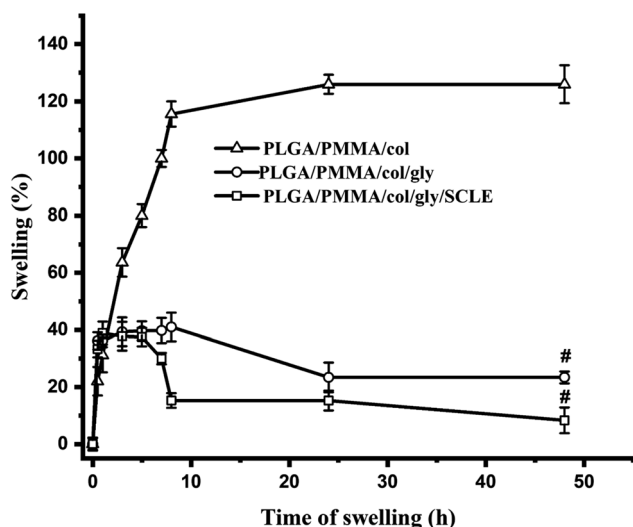


Fig. 6 Swelling ratio of electrospun PLGA/PMMA/col/gly/SCLE nanofibers was measured at various time intervals between 0 and 12 hours. The results, presented as the mean  $\pm$  standard deviation ( $n = 3$ ). # refers to statistical difference compared to the untreated group (Group 1) ( $p < 0.0001$ ).

explained by the presence of various groups of bioactive metabolites. Earlier studies identified secondary metabolites (phytochemical substances), such as flavonoids, phenolic compounds, saponins, tannins, anthocyanins and terpenes, as antimicrobial compounds.<sup>61</sup> For example, an earlier study displayed the therapeutic benefit of *S. cumini* extract in treating conditions affecting the oral cavity, including dental caries, periodontitis, dental infections, and yeast infection.<sup>63</sup> *S. cumini* extracts have also demonstrated a variety of biological activities owing to their anti-inflammatory, antioxidant, and anti-carcinogenic effects.<sup>64</sup>

In our investigation, we used agar-well diffusion to assess the antimicrobial efficacy of our formulations against multidrug-resistant human pathogens. By examining the presence or absence of inhibitory zones, antimicrobial activity was evaluated. The diameter of the region that showed no microbial

growth was then measured as shown in Table 4. The results (Fig. 7G) show that formulations containing 0.5% (F10) or 1% (F11) *S. cumini* extract have higher antimicrobial effectiveness against all tested human pathogens compared to positive controls containing 0.5% (F15) or 1% (F16) *S. cumini* extract. The data shown in Table 4 highlights the effect of the tested formulations on the Gram-positive (Fig. 7A, B) and Gram-negative (Fig. 7C, D) bacterial strains, as well as the tested fungus strains (Fig. 7E and F). As shown in Fig. 7, the data for Gram-negative strains demonstrated that *Salmonella paratyphi* was more sensitive to F10 ( $23.35 \pm 3.78$  mm) compared to F11 ( $16.1 \pm 1.015$  mm). Additionally, the findings demonstrate that *Bacillus cereus*, a Gram-positive bacterium, was more responsive to F11 ( $22.67 \pm 3.21$  mm) compared to F10 ( $14.29 \pm 3.21$  mm). However, F10 was more effective against *Staphylococcus aureus* ( $16.35 \pm 1.53$  mm) than F11 ( $10.71 \pm 1.53$  mm) treatments. On the other hand, as seen in Fig. 7F, *Candida albicans* was more resistant to all formulations that were examined. However, in case of *Candida glabrata* (Fig. 7E), comparable results were obtained using F11 ( $13.33 \pm 4.16$  mm), F10 ( $12.5 \pm 2.17$  mm), and F16 ( $10.47 \pm 1.53$  mm), but the strain was resistant to F15. The antimicrobial effect of the SCLE-loaded NFs can be attributed to the phenolic and flavonoid components of *S. cumini* extract that can reduce membrane permeability by accumulating on cell membranes. After that, the protein structure of microbial cells might entirely degrade and leak which could result in cell death.<sup>61</sup>

### 3.7 In vitro cytotoxicity test

In vitro cytotoxicity test of the prepared extract-loaded NFs and other components of the NFs (*i.e.*, PLGA, PMMA, SCLE, collagen) were evaluated and shown in Fig. 8. SCLE showed an increase in the cytotoxicity of Vero cells in a dose-dependent manner (*i.e.*, 75% at concentration of  $0.1 \text{ mg mL}^{-1}$  and *ca.* 23.5% at concentration of  $0.8 \text{ mg mL}^{-1}$ ). However, cytotoxicity decreased by using SCLE in PLGA/PMMA/col/gly scaffolds. Cells treated with collagen, PLGA, and PMMA demonstrated no cytotoxicity at all tested concentrations, however, cell viability

Table 4 The measured inhibitory zone sizes (mm  $\pm$  SD) that developed when our tested formulations were used for fighting human pathogens<sup>a</sup>

Formulations	Diameter of zone inhibition (mm $\pm$ SD)					
	<i>Salmonella paratyphi</i>	<i>Escherichia coli</i>	<i>Staphylococcus aureus</i>	<i>Bacillus cereus</i>	<i>Candida glabrata</i>	<i>Candida albicans</i>
F6	0	0	0	0	0	0
F7	0	0	0	0	0	0
F8	0	0	0	0	0	0
F9	0	0	0	0	0	0
F10	$23.35 \pm 3.78$	$9.0 \pm 3.61$	$16.35 \pm 1.53$	$14.29 \pm 3.21$	$12.5 \pm 2.17$	0
F11	$16.1 \pm 1.015$	$14.83 \pm 2.36$	$10.71 \pm 1.53$	$22.67 \pm 3.21$	$13.33 \pm 4.16$	0
F12	0	0	0	0	0	0
F13	0	0	0	0	0	0
F14	0	0	0	0	0	0
F15	$5.53 \pm 3.62$	$3.17 \pm 0.76$	0	0	0	0
F16	$5.45 \pm 0.57$	$6.45 \pm 3.89$	$5.04 \pm 2.06$	$13.12 \pm 2.49$	$10.47 \pm 1.53$	0

<sup>a</sup> SD = Standard deviation.



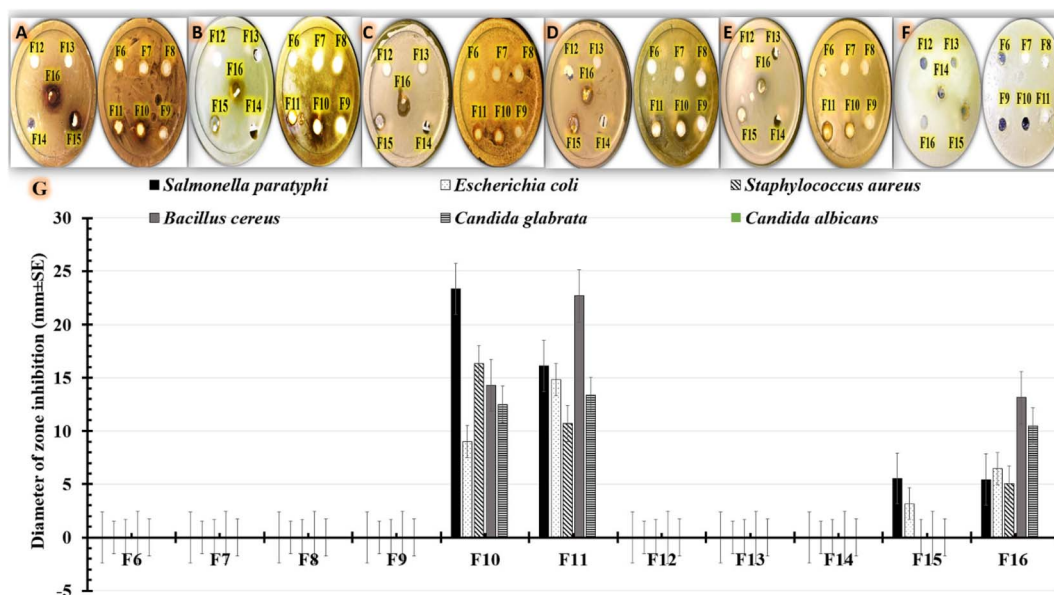


Fig. 7 Photographs and a chart show the measured inhibitory zone widths (mm ± SE) that were observed when our formulations (F6, F7, F8, F9, F10, F11, F12 (15% PLGA), F13 (10% PMMA), F14 (1% collagen), F15, and F16) were applied to inhibit the growth of human infections; (A) *Salmonella paratyphi*, (B) *Escherichia coli*, (C) *Staphylococcus aureus*, (D) *Bacillus cereus*, (E) *Candida glabrata*, and (F) *Candida albicans*. SE = standard error.

was reduced upon utilizing higher concentrations. Interestingly, the cell viability was increased from 114.7% in F7 to 122.9% in F9 upon increasing the concentration of glycine.

### 3.8 In vivo wound closure assay

According to reported findings of Singla *et al.*, a dressing made from *S. cumini* leaves improved tissue repair by

decreasing inflammation, increasing angiogenesis, speeding up neo-epithelialization, and depositing collagen in mice.<sup>63</sup> Three animal groups were used for this study. Group 1 was treated with cotton gauze and served as a control, group 2 was treated with F7, and group 3 was treated with F11 (Fig. 9). As shown in Fig. 10, on day 3, the F11-treated group demonstrated 26% wound closure, while the control group treated

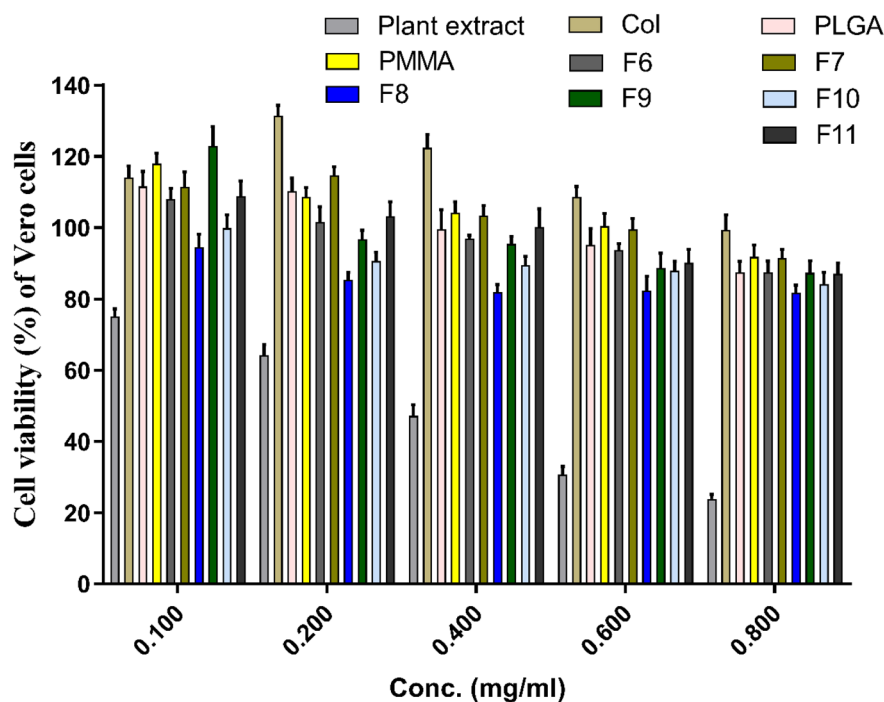


Fig. 8 Cytotoxic assay of the prepared nanofibers against Vero cells after treatment for 72 h. Cytotoxicity of the initial ingredients of SCLE, collagen, PLGA, and PMMA were also evaluated.





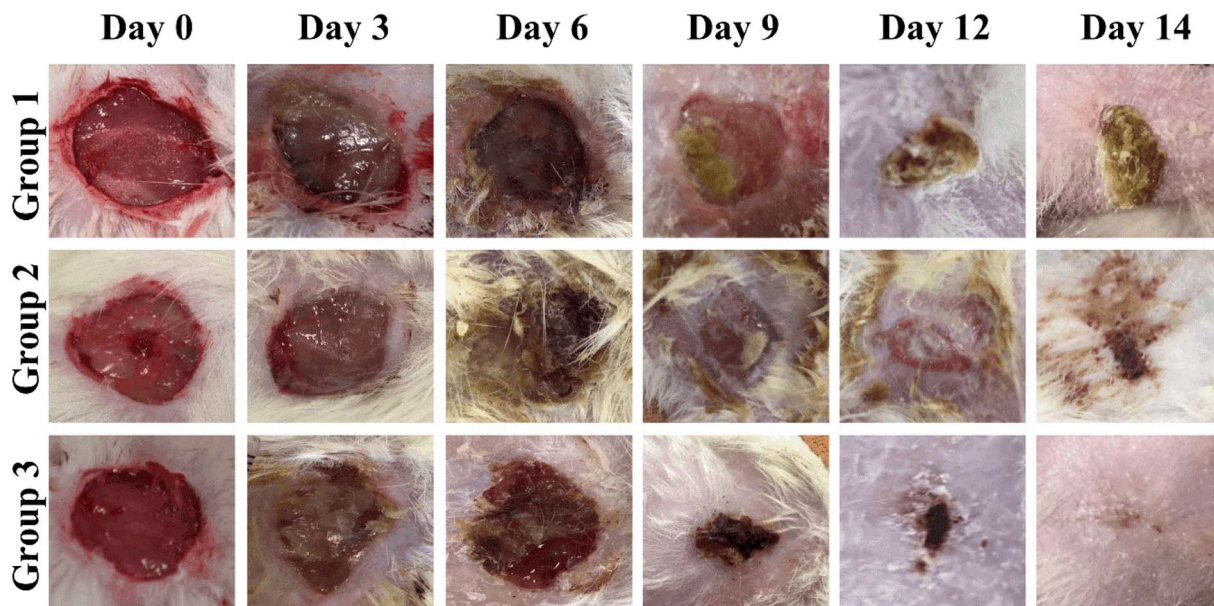


Fig. 9 Representative pictures of skin wounds at various time points (days 0–14) illustrating the effects of nanofibers (NFs) on *in vivo* wound healing. The groups examined include group 1 (control), group 2 (PLGA/PMMA/col/gly (F7)), and group 3 (PLGA/PMMA/col/gly/SCLE (F11)).

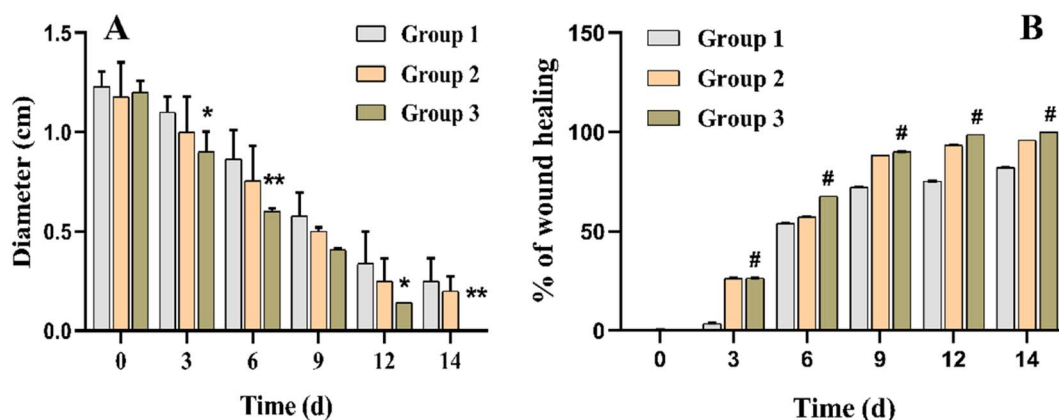


Fig. 10 *In vivo* wound healing results. (A) Wound diameter measurements at 0, 3, 6, 9, 12, and 14 days for different experimental groups. (B) Percentage healing of *in vivo* wounds at 0, 3, 6, 9, 12, and 14 days after creating a full-thickness skin wound. \*, \*\*, # refer to statistical differences compared to the untreated group (Group 1) at  $p < 0.01$ ,  $p < 0.001$  and  $p < 0.0001$ , respectively.

with cotton gauze displayed only 3.5% wound closure (Fig. 10B). Animals treated with F7, and F11 NFs showed remarkable wound healing, with full closure occurring between days 12 and 14, as compared to the control group. Comparatively, the time needed for complete re-epithelialization to occur in the control group was longer than 14 days. The synergistic impact of SCLE in the F11 scaffold, led to faster wound healing, evidenced by the statistically remarkable alteration in wound closure among the control group, F7 and F11 groups (Fig. 9). Thus, SCLE-loaded NFs (F11) displayed superior wound healing activity as compared to untreated or unloaded NFs groups.

### 3.9 Histopathological analysis

Sections in skin wound of control group showed features of lack or delayed wound healing in the form of complete absence of collagen fibres and scar formation (stage 3 and 4), with complete epithelial ulceration covered by fibrino-purulent exudate with underlying granulation tissue and neovascularization with no evidence of collagen fibres (Fig. 11A–C). Fig. 11D showed evidence of early onset of collagen fibres formation (stage 3), but with random orientation, not parallel to surface epithelium. Sections of the wound of nanofiber-treated group showed evidence of adequate wound healing in the form of organized scar (stage 4) collagen





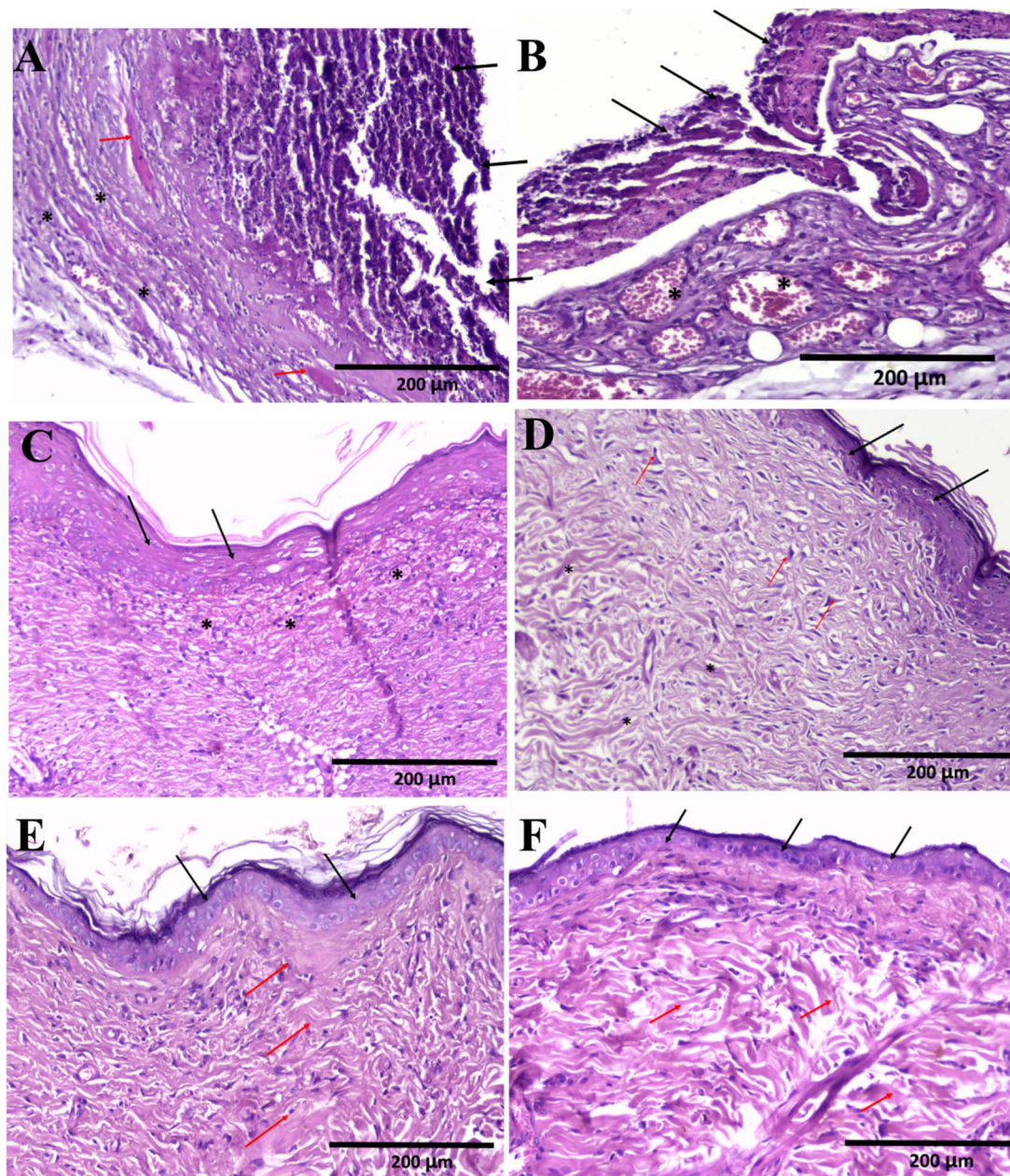


**Fig. 11** Histopathology of wound healing in control and NFs-treated skin wounds. (A) Section in skin wound in control group showing complete epithelial ulceration covered by fibrinopurulent exudate (black arrows) with underlying granulation tissue and neovascularization (\*) with few scattered collagen fibers (red arrows) H&E  $\times$  200. (B) Section in skin wound in control group showing complete epithelial ulceration covered by fibrinopurulent exudate (black arrows) with underlying granulation tissue and neovascularization (\*) with no evidence of collagen fibers. H&E  $\times$  200. (C) Section from wound in control group covered by regenerating attenuated squamous epithelium (black arrows) with underlying granulation and neovascularization (\*). No evidence of collagen bands. H&E  $\times$  200. (D) Section from wound in control group covered by regenerating attenuated squamous epithelium (black arrows) with underlying maturing granulation tissue showing prominent fibroblasts (red arrows). Creeping collagen fibers with haphazard orientation are noted from deep dermis (\*). H&E  $\times$  200. (E) Section in wound of nanofiber treated with F11 group showing complete epithelial recovery (black arrows). The underlying dermis shows well-formed collagen bands with organized parallel orientation to the surface epithelium and scar formation (red arrows) with complete replacement of granulation tissue indicating complete recovery. H&E  $\times$  200. (F) Section in wound of nanofiber treated with F11 group showing complete epithelial recovery (black arrows). The underlying dermis shows well-formed collagen bands with organized parallel orientation to the surface epithelium (red arrows) with complete replacement of granulation tissue indicating complete recovery. H&E  $\times$  200.

fibres formation (stage 3) parallel to epithelial surface with complete epithelial recovery and complete replacement of granulation tissue showing complete epithelial recovery (Fig. 11E and F).

## 4 Conclusions

SCLE-loaded NFs were successfully prepared *via* electro-spinning and were assessed *in vitro* and *in vivo*. The optimized



SCLE-loaded NFs exhibited nanosized and uniform fibers. The optimized NFs had antibacterial activity particularly after loading the SCLE. Also, *in vivo*, animals treated with SCLE-loaded NFs displayed significant wound healing properties over 14 days compared to the untreated group and the group treated with SCLE only. Thus, the fabricated NFs loaded with SCLE could be employed as an effective biocompatible antimicrobial and wound healing composites for management of acute wounds and injuries.

## Ethical statement

All research studies followed the Helsinki World Medical Association's Declaration: Ethical Medical Research Principles Involving Human Subjects. The *in vivo* experimental procedures were reviewed and approved by Badr University in Cairo-Institutional Ethical Committee (BUC-IACUC-230507-19).

## Conflicts of interest

The authors declare that they have no conflict of interest.

## References

- 1 A. Y. M. Alabdali, R. Khalid, M. Kzar, M. O. Ezzat, G. M. Huei, T. W. Hsia, R. Mogana, H. Rahman, B. M. A. Razik, P. K. Issac, S. Chinnappan and S. I. Khalivulla, Design, synthesis, *in silico* and antibacterial evaluation of curcumin derivatives loaded nanofiber as potential wound healing agents, *J. King Saud Univ., Sci.*, 2022, **34**, 102205, DOI: [10.1016/j.jksus.2022.102205](#).
- 2 J. R. Dias, P. L. Granja and P. J. Bártolo, Advances in electrospun skin substitutes, *Prog. Mater. Sci.*, 2016, **84**, 314–334, DOI: [10.1016/j.pmatsci.2016.09.006](#).
- 3 M. Elsabahy, G. S. Heo, S. M. Lim, G. Sun and K. L. Wooley, Polymeric Nanostructures for Imaging and Therapy, *Chem. Rev.*, 2015, **115**, 10967–11011, DOI: [10.1021/acs.chemrev.5b00135](#).
- 4 C. H. Yao, K. Y. Chen, Y. S. Chen, S. J. Li and C. H. Huang, Lithospermum radix extract-containing bilayer nanofiber scaffold for promoting wound healing in a rat model, *Mater. Sci. Eng., C*, 2019, **96**, 850–858, DOI: [10.1016/j.msec.2018.11.053](#).
- 5 M. Elsabahy, M. Zhang, S. M. Gan, K. C. Waldron and J. C. Leroux, Synthesis and enzymatic stability of PEGylated oligonucleotide duplexes and their self-assemblies with polyamidoamine dendrimers, *Soft Matter*, 2008, **4**, 294, DOI: [10.1039/b714221h](#).
- 6 S. Samarajeewa, A. Ibricevic, S. P. Gunsten, R. Shrestha, M. Elsabahy, S. L. Brody and K. L. Wooley, Degradable cationic shell cross-linked knedel-like nanoparticles: synthesis, degradation, nucleic acid binding, and *in vitro* evaluation, *Biomacromolecules*, 2013, **14**, 1018–1027, DOI: [10.1021/bm3018774](#).
- 7 F. Zhang, S. Khan, R. Li, J. A. Smolen, S. Zhang, G. Zhu, L. Su, A. A. Jahnke, M. Elsabahy, X. Chen and K. L. Wooley, Design and development of multifunctional polyphosphoester-based nanoparticles for ultrahigh paclitaxel dual loading, *Nanoscale*, 2017, **9**, 15773–15777, DOI: [10.1039/c7nr05935c](#).
- 8 S. N. Nandhini, N. Sisubalan, A. Vijayan, C. Karthikeyan, M. Gnanaraj, D. A. M. Gideon, T. Jebastin, K. Varaprasad and R. Sadiku, Recent advances in green synthesized nanoparticles for bactericidal and wound healing applications, *Heliyon*, 2023, **9**, e13128, DOI: [10.1016/j.heliyon.2023.e13128](#).
- 9 T. Gulsun, M. Inal, Y. Akdag, N. Izat, L. Oner and S. Sahin, The development and characterization of electrospun gelatin nanofibers containing indomethacin and curcumin for accelerated wound healing, *J. Drug Delivery Sci. Technol.*, 2022, **67**, 103000, DOI: [10.1016/j.jddst.2021.103000](#).
- 10 M. A. Shahid, M. S. Khan and M. M. Hasan, Licorice extract-infused electrospun nanofiber scaffold for wound healing, *OpenNano*, 2022, **8**, 100075, DOI: [10.1016/j.onano.2022.100075](#).
- 11 J. Grip, R. E. Engstad, I. Skjæveland, N. Škalko-Basnet, J. Isaksson, P. Basnet and A. M. Holsæter, Beta-glucan-loaded nanofiber dressing improves wound healing in diabetic mice, *Eur. J. Pharm. Sci.*, 2018, **121**, 269–280, DOI: [10.1016/j.ejps.2018.05.031](#).
- 12 H. A. Fathi, A. Abdelkader, M. S. AbdelKarim, A. A. Abdelaziz, M. A. El Mokhtar, A. Allam, G. Fetih, M. El Badry and M. Elsabahy, Electrospun vancomycin-loaded nanofibers for management of methicillin-resistant *Staphylococcus aureus*-induced skin infections, *Int. J. Pharm.*, 2020, **586**, 119620, DOI: [10.1016/j.ijpharm.2020.119620](#).
- 13 B. S. Alotaibi, M. Shoukat, M. Buabeid, A. K. Khan and G. Murtaza, Healing potential of neomycin-loaded electrospun nanofibers against burn wounds, *J. Drug Delivery Sci. Technol.*, 2022, **74**, 103502, DOI: [10.1016/j.jddst.2022.103502](#).
- 14 N. Badrinath, Y. Il Jeong, H. Y. Woo, S. Y. Bang, C. Kim, J. Heo, D. H. Kang and S. Y. Yoo, Local delivery of a cancer-favoring oncolytic vaccinia virus via poly (lactic-co-glycolic acid) nanofiber for theranostic purposes, *Int. J. Pharm.*, 2018, **552**, 437–442, DOI: [10.1016/j.ijpharm.2018.10.020](#).
- 15 E. Gomaa, N. G. Eissa, T. M. Ibrahim, H. M. El-Bassossy, H. M. El-Nahas and M. M. Ayoub, Development of depot PLGA-based *in-situ* implant of Linagliptin: sustained release and glycemic control, *Saudi Pharm. J.*, 2023, **31**, 499–509, DOI: [10.1016/j.jsps.2023.02.002](#).
- 16 H. Taghiyar, B. Yadollahi, S. J. Moshtaghian, A. Talebi and A. Abbasi Kajani, PMMA nanofibers containing Keplerate-type polyoxometalate and metronidazole: preparation and wound-healing effect in a rat model, *J. Drug Delivery Sci. Technol.*, 2022, **69**, 103140, DOI: [10.1016/j.jddst.2022.103140](#).
- 17 J. X. Law, F. Musa, B. H. I. Ruszymah, A. J. El Haj and Y. Yang, A comparative study of skin cell activities in collagen and fibrin constructs, *Med. Eng. Phys.*, 2016, **38**, 854–861, DOI: [10.1016/j.medengphy.2016.05.017](#).
- 18 F. R. Saber, P. E. S. Munekata, K. Rizwan, H. A. S. El-nashar, N. M. Fahmy, S. H. Aly, M. El-shazly, A. Bouyahya and J. M. Lorenzo, Family Myrtaceae: the treasure hidden in





- the complex/diverse composition, *Crit. Rev. Food Sci. Nutr.*, 2023, 1–19, DOI: [10.1080/10408398.2023.2173720](https://doi.org/10.1080/10408398.2023.2173720).
- 19 K. A. Reynertson, M. J. Basile and E. J. Kennelly, Antioxidant potential of seven myrtaceous fruits, *Ethnobot. Res. Appl.*, 2005, 3, 25–36.
  - 20 G. Balakrishna, K. Sowmya, V. R. Bollapalli and M. R. Rao, Anti-allergic studies of *Alibizzia Lebbeck* and *Syzygium cumini* (L. *Syzygium gambolana*), *J. Microbiol. Biotechnol.*, 2016, 1, 103.
  - 21 S. Srivastava and D. Chandra, Pharmacological potentials of *Syzygium cumini*: a review, *J. Sci. Food Agric.*, 2013, 93, 2084–2093.
  - 22 S. A. J. Kazmi, A. Riaz, N. Akhter and R. A. Khan, Evaluation of wound healing effects of *Syzygium cumini* and laser treatment in diabetic rats, *Pak. J. Pharm. Sci.*, 2020, 33, 779–786.
  - 23 S. J. Liu, Y. C. Kau, C. Y. Chou, J. K. Chen, R. C. Wu and W. L. Yeh, Electrospun PLGA/collagen nanofibrous membrane as early-stage wound dressing, *J. Membr. Sci.*, 2010, 355, 53–59, DOI: [10.1016/j.memsci.2010.03.012](https://doi.org/10.1016/j.memsci.2010.03.012).
  - 24 S. H. Aly, A. M. Elissawy, A. M. A. Mahmoud, F. S. El-tokhy, S. S. A. Mageed, H. Almahli, S. T. Al-rashood, F. A. Binjubair, M. A. El Hassab, W. M. Eldehna and A. E. B. Singab, Synergistic Effect of *Sophora japonica* and *Glycyrrhiza glabra* Flavonoid-Rich Fractions on Wound Healing: In Vivo and Molecular Docking Studies, *Molecules*, 2023, 28, 2994.
  - 25 S. H. Aly, A. M. Elissawy, D. Salah, N. A. Alfuhaid, O. H. Zyaan, H. I. Mohamed, A. N. B. Singab and S. M. Farag, Phytochemical Investigation of Three *Cystoseira* Species and Their Larvicidal Activity Supported with In Silico Studies, *Mar. Drugs*, 2023, 1–17.
  - 26 S. A. Salim, E. A. Kamoun, S. Evans, T. H. Taha, E. M. El-Fakharany, M. M. Elmazar, A. F. Abdel-Aziz, R. H. Abou-Saleh and T. A. Salaheldin, Novel oxygen-generation from electrospun nanofibrous scaffolds with anticancer properties: synthesis of PMMA-conjugate PVP-H<sub>2</sub>O<sub>2</sub> nanofibers, characterization, and: in vitro bio-evaluation tests, *RSC Adv.*, 2021, 11, 19978–19991, DOI: [10.1039/d1ra02575a](https://doi.org/10.1039/d1ra02575a).
  - 27 N. A. Al-Dhabi, A. K. M. Ghilan, M. V. Arasu and V. Duraipandian, Green biosynthesis of silver nanoparticles produced from marine *Streptomyces* sp. Al-Dhabi-89 and their potential applications against wound infection and drug resistant clinical pathogens, *J. Photochem. Photobiol., B*, 2018, 189, 176–184, DOI: [10.1016/j.jphotobiol.2018.09.012](https://doi.org/10.1016/j.jphotobiol.2018.09.012).
  - 28 T. Mirmajidi, F. Chogan, A. H. Rezayan and A. M. Sharifi, In vitro and in vivo evaluation of a nanofiber wound dressing loaded with melatonin, *Int. J. Pharm.*, 2021, 596, 120213, DOI: [10.1016/j.jipharm.2021.120213](https://doi.org/10.1016/j.jipharm.2021.120213).
  - 29 M. K. Heljak, E. Kijeńska-Gawrońska, A. Chlanda, M. Łojkowski, J. Jaroszewicz, C. de Maria, G. Vozzi and W. Swieszkowski, High-resolution microscopy assisted mechanical modeling of ultrafine electrospun network, *Polymer*, 2021, 230, 124050, DOI: [10.1016/j.polymer.2021.124050](https://doi.org/10.1016/j.polymer.2021.124050).
  - 30 S. E. Moghadam, S. N. Ebrahimi, P. Salehi, M. M. Farimani, M. Hamburger and E. Jabbarzadeh, Wound healing potential of chlorogenic acid and myricetin-3-o- $\beta$ -rhamnoside isolated from *parrotia persica*, *Molecules*, 2017, 22, 1–15, DOI: [10.3390/molecules22091501](https://doi.org/10.3390/molecules22091501).
  - 31 A. I. Elshamy, N. M. Ammar, H. A. Hassan, W. A. El-Kashak, S. S. Al-Rejaie, A. M. Abd-ElGawad and A. R. H. Farrag, Topical wound healing activity of myricetin isolated from *tecomaria capensis* v. *aurea*, *Molecules*, 2020, 25, 1–13, DOI: [10.3390/molecules25214870](https://doi.org/10.3390/molecules25214870).
  - 32 Y. Özey, S. Güzel, Ö. Yumrutaş, B. Pehlivanoğlu, İ. H. Erdoğan, Z. Yildirim, B. A. Türk and S. Darcan, Wound healing effect of kaempferol in diabetic and nondiabetic rats, *J. Surg. Res.*, 2019, 233, 284–296, DOI: [10.1016/j.jss.2018.08.009](https://doi.org/10.1016/j.jss.2018.08.009).
  - 33 P. Lopez-Jornet, F. Camacho-Alonso, F. Gómez-García, F. Molina Miñano, X. Cañas, A. Serafín, J. Castillo and V. Vicente-Ortega, Effects of potassium apigenin and verbena extract on the wound healing process of SKH-1 mouse skin, *Int. Wound J.*, 2014, 11, 489–495, DOI: [10.1111/j.1742-481X.2012.01114.x](https://doi.org/10.1111/j.1742-481X.2012.01114.x).
  - 34 A. Rajab, W. Al-Wattar and G. A. Taqa, The Roles of Apigenin Cream on Wound Healing in Rabbits Model, *J. Appl. Vet. Sci.*, 2022, 7, 1–5, DOI: [10.21608/javs.2021.97151.1104](https://doi.org/10.21608/javs.2021.97151.1104).
  - 35 M.-Q. Man, M. Hupe, R. Sun, G. Man, T. M. Mauro and P. M. Elias, Topical apigenin alleviates cutaneous inflammation in murine models, Evidence-Based Complement, *Altern. Med.*, 2012, 1–7.
  - 36 S. A. Aslam, I. Khan, F. Jameel and M. B. Zaidi, Umbilical cord-derived mesenchymal stem cells preconditioned with isorhamnetin: potential therapy for burn wounds, *World J. Stem Cells*, 2020, 12, 1652.
  - 37 L. Xu, T. H. Choi, S. Kim, S. H. Kim, H. W. Chang, M. Choe, S. Y. Kwon, J. A. Hur, S. C. Shin, J. Il Chung, D. Kang and D. Zhang, Anthocyanins from black soybean seed coat enhance wound healing, *Ann. Plast. Surg.*, 2013, 71, 415–420, DOI: [10.1097/SAP.0b013e31824ca62b](https://doi.org/10.1097/SAP.0b013e31824ca62b).
  - 38 M. C. Raharisoa, C. Rasolohery, N. Tombozara, D. Ramanitrahassimbola, R. S. Andriantiaray, B. Bodo and M. Rakotovaio, Lignans from the seeds of *Brochoneura acuminata* (Myristicaceae) and the antioxidant and wound healing properties of the methanol extract, *J. Pharmacogn. Phytochem.*, 2021, 10, 104–109.
  - 39 A. Z. Tulio Jr, C. Chang, I. Edirisinghe, K. D. White, J. E. Jablonski, K. Banaszewski, A. Kangath, R. K. Tadapaneni, B. Burton-Freeman and L. S. Jackson, Berry fruits modulated endothelial cell migration and angiogenesis via phosphoinositide-3 kinase/protein kinase B pathway in vitro in endothelial cells, *J. Agric. Food Chem.*, 2012, 60, 5803–5812.
  - 40 K. S. De Bona, G. Bonfanti, P. E. R. Bitencourt, T. P. da Silva, R. M. Borges, A. Boligon, A. Pigatto, M. L. Athayde and M. B. Moretto, Protective effect of gallic acid and *Syzygium cumini* extract against oxidative stress-induced cellular injury in human lymphocytes, *Drug Chem. Toxicol.*, 2016, 39, 256–263.





- 41 H. Sagrawat, A. Mann and M. Kharya, Pharmacological potential of *Eugenia jambolana*: a review, *Pharmacogn. Mag.*, 2006, **2**, 96–105.
- 42 K. Alagesan, P. Thennarasu, V. Kumar, S. Sankarnarayanan and T. Balsamy, Identification of  $\alpha$ -glucosidase inhibitors from *Psidium guajava* leaves and *Syzygium cumini* Linn. seeds, *Int. J. Pharma Sci. Res.*, 2012, **3**, 316–322.
- 43 S. S. Subramanian and A. G. R. Nair, Flavonoids of the flowers of *Eugenia jambolana*, *Curr. Sci.*, 1972, **41**, 703–704.
- 44 G. Venkateswarlu, On the nature of the colouring matter of the jambu fruit (*Eugenia-jambolana*), *J. Indian Chem. Soc.*, 1952, **29**, 434–437.
- 45 S. Ramya, K. Neethirajan and R. Jayakumararaj, Profile of bioactive compounds in *Syzygium cumini*-a review, *J. Pharma Res.*, 2012, **5**, 4548–4553.
- 46 Y. S. Lewis, C. T. Dwarakanath and D. S. Johar, Acids and sugars in *Eugenia jambolana*, *J. Sci. Ind. Res.*, 1956, **15**, 280–281.
- 47 I. I. Mahmoud, M. S. A. Marzouk, F. A. Moharram, M. R. El-Gindi and A. M. K. Hassan, Acylated flavonol glycosides from *Eugenia jambolana* leaves, *Phytochemistry*, 2001, **58**, 1239–1244.
- 48 T. S. Martin, K. Ohtani, R. Kasai and K. Yamasaki, Lignan glucoside from *Syzygium cumini*, *Nat. Med.*, 1998, **52**, 360–363.
- 49 T. C. M. De Lima, P. A. Klüeger, P. A. Pereira, W. P. Macedo-Neto, G. S. Morato and M. R. Farias, Behavioural effects of crude and semi-purified extracts of *Syzygium cumini* linn. skeels, *Phytother. Res.*, 1998, **12**, 488–493.
- 50 N. M. Nazif, The anthocyanin components and cytotoxic activity of *Syzygium cumini* (L.) fruits growing in Egypt, *Nat. Prod. Sci.*, 2007, **13**, 135–139.
- 51 M. Ayyanar and P. Subash-Babu, *Syzygium cumini* (L.) Skeels: a review of its phytochemical constituents and traditional uses, *Asian Pac. J. Trop. Biomed.*, 2012, **2**, 240–246.
- 52 E. E. Aung, A. N. Kristanti, N. S. Aminah, Y. Takaya and R. Ramadhan, Plant description, phytochemical constituents and bioactivities of *Syzygium* genus: a review, *Open Chem.*, 2020, **18**, 1256–1281.
- 53 E. S. Lago, E. Gomes and R. da Silva, *Extraction and Anthocyanic Pigment Quantification of the Jamun Fruit (Syzygium cumini Lamark)*, 2004.
- 54 Q. Y. Mir, M. Ali and P. Alam, Lignan derivatives from the stem bark of *Syzygium cumini* (L.) Skeels, *Nat. Prod. Res.*, 2009, **23**, 422–430.
- 55 P. Huo, X. Han, W. Zhang, J. Zhang, P. Kumar and B. Liu, Electrospun nanofibers of polycaprolactone/collagen as a sustained-release drug delivery system for artemisinin, *Pharmaceutics*, 2021, **13**(8), 1228, DOI: [10.3390/pharmaceutics13081228](https://doi.org/10.3390/pharmaceutics13081228).
- 56 D. Miele, L. Catenacci, S. Rossi, G. Sandri, M. Sorrenti, A. Terzi, C. Giannini, F. Riva, F. Ferrari, C. Caramella and M. C. Bonferoni, Collagen/PCL Nanofibers Electrospun in Green Solvent by DOE Assisted Process. An Insight into Collagen Contribution, *Materials*, 2020, **13**, 4–6.
- 57 A. Guzmán-Soria, V. Moreno-Serna, D. A. Canales, C. García-Herrera, P. A. Zapata and P. A. Orihuela, Effect of Electrospun PLGA/Collagen Scaffolds on Cell Adhesion, Viability, and Collagen Release: Potential Applications in Tissue Engineering, *Polymer*, 2023, **15**, 1079, DOI: [10.3390/POLYM15051079](https://doi.org/10.3390/POLYM15051079).
- 58 S. F. Fatima, S. Ishtiaq, M. O. Lashkar, F. S. Youssef, M. L. Ashour and S. S. Elhady, Metabolic Profiling of *Heliotropium crispum* Aerial Parts Using HPLC and FTIR and In Vivo Evaluation of Its Anti-Ulcer Activity Using an Ethanol Induced Acute Gastric Ulcer Model, *Metabolites*, 2022, **12**(8), 750, DOI: [10.3390/metabo12080750](https://doi.org/10.3390/metabo12080750).
- 59 D. D. Giri, A. Alhazmi, A. Mohammad, S. Haque, N. Srivastava, V. K. Thakur, V. K. Gupta and D. B. Pal, Lead removal from synthetic wastewater by biosorbents prepared from seeds of *Artocarpus Heterophyllus* and *Syzygium Cumini*, *Chemosphere*, 2022, **287**, 132016, DOI: [10.1016/j.chemosphere.2021.132016](https://doi.org/10.1016/j.chemosphere.2021.132016).
- 60 S. Khanal, U. Adhikari, N. P. Rijal, S. R. Bhattarai, J. Sankar and N. Bhattarai, pH-Responsive PLGA Nanoparticle for Controlled Payload Delivery of Diclofenac Sodium, 2016, DOI: [10.3390/jfb7030021](https://doi.org/10.3390/jfb7030021).
- 61 E. C. Figueirêdo Júnior, B. P. Costa, J. C. P. Freire, W. O. d. S. Melo, C. R. Ferreira de Araújo, E. M. M. d. B. Costa and J. V. Pereira, Therapeutic applications and antibacterial and antifungal activities of *Syzygium cumini* (L.) Skeels extracts: a systematized literature review focusing on dental applications, *Arch. Health Investig.*, 2021, **10**, 547–553, DOI: [10.21270/archi.v10i4.4841](https://doi.org/10.21270/archi.v10i4.4841).
- 62 R. Haque, M. K. Sumiya, N. Sakib, O. S. Sarkar, T. T. I. Siddique, S. Hossain, A. Islam, A. K. Parvez, A. A. Talukder and S. K. Dey, Antimicrobial Activity of Jambul (*Syzygium cumini*) Fruit Extract on Enteric Pathogenic Bacteria, *Adv. Microbiol.*, 2017, **7**, 195–204, DOI: [10.4236/aim.2017.73016](https://doi.org/10.4236/aim.2017.73016).
- 63 R. Singla, S. Soni, V. Patial, P. M. Kulurkar, A. Kumari, S. Mahesh, Y. S. Padwad and S. K. Yadav, Cytocompatible Anti-microbial Dressings of *Syzygium cumini* Cellulose Nanocrystals Decorated with Silver Nanoparticles Accelerate Acute and Diabetic Wound Healing, *Sci. Rep.*, 2017, **7**, 1–13, DOI: [10.1038/s41598-017-08897-9](https://doi.org/10.1038/s41598-017-08897-9).
- 64 N. Azzaz, S. Hamed and A. Mohamed, Antimicrobial and Anticancer Activities of *Syzygium cumini* Extracts, *J. Agric. Chem. Biotechnol.*, 2022, **13**, 35–38, DOI: [10.21608/jacb.2022.118330.1017](https://doi.org/10.21608/jacb.2022.118330.1017).

